AD-A161 912 AN INVESTIGATION OF SYNTHETIC APERTURE RADAR AUTOFOCUS (U) ROYAL SIGNALS AND RADAR ESTABLISHMENT CHRISTCHURCH (ENGLAND) I P FINLEY ET AL. APR 85 RSRE-MEMO-3780 1/1

UNCLASSIFIED DRIC-BR-97350 F/G 17/9 NL

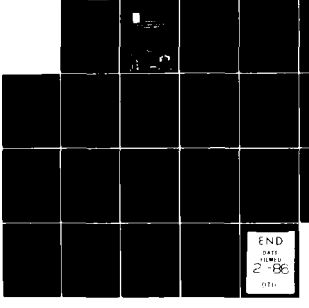

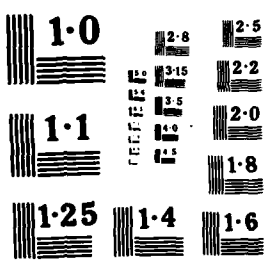
1·0
1·1
1·25
2·8
3·15
3·5
4·0
2·5
2·2
2·0
1·8
1·4
1·6

[redacted]

[redacted]

ROYAL SIGNALS & RADAR ESTABLISHMENT

[redacted]

ROYAL SIGNALS AND RADAR ESTABLISHMENT

Memorandum 3790

Title: AN INVESTIGATION OF SYNTHETIC APERTURE RADAR AUTOFOCUS

Authors: I P Finley and J W Wood

Date: April 1985

SUMMARY

SAR imagery is generated by matched filtering the raw azimuth signal history, assuming uniform straight line motion of the aircraft. Unknown aircraft motions alter the matched filter required for processing. Autofocussing involves determining from the raw data the appropriate matched filter.

In this ~~memorandum~~ the principles of SAR and the requirement for an autofocus system are discussed. Three autofocus methods are investigated: measurement of the power spectrum, contrast maximisation, and registration of multilook images. The power spectrum is shown to be unreliable as an autofocus aid. Results of the contrast maximisation and registration methods are compared.

RSRE MEMORANDUM 3790

AN INVESTIGATION OF SAR AUTOFOCUS

I P Finley and J W Wood

CONTENTS

1 INTRODUCTION

The RSRE X-band SAR is a system theoretically capable of producing image data at a nominal resolution of several metres in azimuth and range, at ranges of 10's of km, given a sufficiently stable platform. Range resolution is achieved using on-board pulse-compression techniques, while azimuth processing is currently done at RSRE on a Marconi hardware processor.

The Sensor Information Processing section of BS1 division has recently developed a software processor, which can process data to produce imagery at any desired nominal azimuth resolution. Whilst operating this processor at high resolution, it became apparent that the system was subject to defocussing errors, which were sometimes so severe as to render the image useless for any further processing. This memorandum describes work done to correct these defocus errors.

Section 2 briefly introduces the principles of SAR. The effects of non-uniform aircraft motion on the quality and geometry of the processed image are discussed in section 3. Section 4 derives the conditions for correctly focussed images.

In the next three sections, methods of focussing the images are examined. Section 5 describes how measurement of the power spectrum of the raw data may be expected to lead to an autofocus method, and the problems encountered in using it. In sections 6 and 7, two methods based on properties of the processed image are presented. In section 6, focussing by maximising the contrast in the processed image is discussed. The other method, based on the misregistration of defocussed multilook images, is described in section 7. Section 8 compares the results obtained from the two methods. The conclusions are presented in section 9.

2 PRINCIPLES OF SAR

This section is designed to provide a short introduction to synthetic aperture radar (SAR) with the aim of introducing those concepts necessary to understanding the basis of autofocussing.

Synthetic aperture radar is a technique for enhancing azimuth (along-track) resolution to a much finer level than the real beamwidth that illuminates the terrain. The basic geometry of the aircraft and single scatterer is shown in Fig 1. The aircraft radar emits pulses at fixed intervals along the flight path, and the propagation time of each pulse to the scatterer and back determines the range of the scatterer. This is no different from a conventional radar and we may assume that the signal return from a single emitted pulse has been divided in time and allocated to the appropriate range bin. However, the range of a scatterer from the aircraft varies slightly with distance along the flight path, being more distant when the scatterer is entering or leaving the beam and closest when the scatterer is broadside. For aircraft SAR (as opposed to satellite-borne SAR) this variation in range along-track is less than the range resolution which ensures that the scatterer signal history does not traverse range bins. The synthetic aperture radar technique relies on detecting this small along-track variation of range in order to more precisely locate the broadside position.

The absolute range of a scatterer within a range cell cannot be determined, but the change of range within a range cell can be measured. Once the returned signal is quantised to a particular range bin, the signal is essentially unchanged in frequency but is shifted in phase relative to the stable oscillator on board the aircraft. The stability of this local oscillator enables phase variation (i.e range variation) to be tracked along the synthetic aperture. The scatterer may approach and recede by many wavelengths, giving a corresponding number of cycles in the phase history.

Processing of the azimuth signal history presumes knowledge of the geometry of the aircraft flight path and the range of the scatterer. Assuming the aircraft flight path to be a straight line, the expected phase history is parabolic. The signal history may be expressed as a complex exponential whose magnitude is proportional to the strength of the scatter and the expression is derived in Fig 2. The signal history is in fact identical to a linear FM chirp. The matched filter required for processing is the complex conjugate of the signal history. A typical matched filter or reference function is shown in Fig 3.

The matched filtering process may be viewed geometrically as a phasor diagram as in Fig 4. The phasor diagram shows a vector sum of successive complex signal returns along track for a single scatterer. The result is a Cornu spiral. One end of the spiral corresponds to the scatterer entering the beam, the centre of the spiral to the broadside position, and the other end to the scatterer leaving the beam. The matched filter, or reference function, is shown as a similar spiral reflected in the real axis. Although the spirals are drawn continuously it consists in practice of sampled points along track (i.e along the spiral) so that the spiral should be drawn as a series of short line segments representing each pulse. If corresponding points on the two curves are multiplied together then the conjugacy of the two numbers ensures a real result. A phasor diagram of all the resulting numbers is a horizontal line whose length is that of the signal Cornu spiral (assuming a normalised reference function). The reference function is shifted to successive azimuth positions to image the scattering strength broadside at those positions. More concisely, digital SAR processing processing is the complex cross-correlation of the complex raw signal and complex reference function as given below:

$$O(p) = (I_{n+p} + jQ_{n+p})(I_{REF_n} + jQ_{REF_n})$$

where $j = \sqrt{-1}$

p = position along track

n = displacement from current position along track

I = raw data, in phase component

Q = raw data, quadrature component

I^{REF} = reference function, real component

Q^{REF} = reference function, imaginary component

O^{REF} = complex processed output

The phase of the scatterer signal broadside may be other than zero, which corresponds to a rotated Cornu spiral. The consequent unwrapping of the spiral by the reference function results in a rotated straight line. Scatterer strength is proportional to the length of the unwrapped spiral therefore the square root of the sum of the squared real and imaginary parts (the modulus) is usually output as the processed image.

The beamwidth associated with a real antenna is inversely proportional to the length of the real antenna. Similarly, the resolution (or synthetic beamwdith) of a synthesised antenna is inversely proportional to the length of the synthetic aperture. If we wish to reduce the resolution of the processed image, the length of the reference function used in the correlation is reduced. If the synthetic aperture length is proportional to range this compensates for the degradation in resolution associated with a real aperture system and gives

a resolution independent of range. The resolution of a SAR system is derived simply in Fig 3. The resolution may also be derived more fundamentally by auto-correlating the reference function and is given by the width of the central peak of the autocorrelation function.

It is worth mentioning that the simple formula of $R\lambda/2.Lsa$ derived in Appendix 1 is slightly optimistic since it assumes uniform illumination. This is not the case towards the edge of the beam, particularly since the amplitude weighting function of the single response is the square of the antenna illumination function. The larger the synthetic aperture, the more important are the effects of attenuation of the edge illumination and the more optimistic the simple formula becomes. At the finest resolution used here the discrepancy is of order of 25%. The naive resolution above can be calibrated to give the actual resolution. Unless stated otherwise, the resolution should be understood to be the naive resolution rather than the actual resolution.

This concludes a brief introduction to the concept of SAR. More detail on SAR can be found in references 1 and 2. To summarise, digital SAR processing is the complex correlation of raw signal and reference function which, from the knowledge of flight path and scatterer geometry is known to be a matched filter.

3 AIRCRAFT MOTION

The previous section emphasised the importance of scatterer and flight path geometry in determining the matched filter. Unfortunately the exact path of an aircraft is uncertain and may deviate significantly from a straight line path. This section briefly describes the effects of different types of aircraft motion.

The distorted geometry due to aircraft motion can be divided into two categories: along-track and across-track. Motion errors across-track are far more serious than errors along-track since they affect the scatterer range (and hence the phase) directly. Along-track and across-track errors can each be sub-divided into errors of position, velocity, acceleration or higher derivatives as described below.

3.1 Across-track Errors

a) Across-track positional error

The only effect is a corresponding shift in the processed range.

b) Across-track velocity

An across-track velocity has no effect on the focussing of the image. It rotates the line of constant range and the broadside locus of zero doppler through the same angle, and it the matched filter processing allocates the zero doppler as the line of constant azimuth (as processed at RSRE), then the net result is a rotation of the image.

c) Across-track acceleration

Across-track acceleration obviously causes image distortion by changing the amount of image rotation along-track, but it is also responsible for defocussing and must be corrected for in the processing. Across-track acceleration combined with uniform motion along-track generates a parabolic trajectory. This imposes an additional quadratic term on the quadratic phase variation derived in the previous section for uniform motion. Acceleration towards a scatterer modifies the scatterer's signal history to a linear

chirp of increased slope, the additional slope being independent of range.

3.2 Along-track Errors

a) Along-track position error

As with across-track position error, the only effect is a corresponding shift in the processed image.

b) Along-track velocity error

If the aircraft is travelling at greater than the desired speed along-track, the spatial interval between the radar pulses is also greater. This has the effect of compressing the parabolic phase history into a smaller number of pulses. A parabolic phase history is equivalent to a linear chirp of constant frequency slope. The effect of an increased aircraft velocity is to generate a linear chirp of increased frequency slope. The modification of signal slope causes defocussing but because the zero-doppler maintains its position broadside there is no image distortion associated with along-track velocity error. However, it does lead to an error in the along-track scale factor of the processed image.

c) Along-track acceleration

Along-track acceleration introduces a cubic term in the signal history, which, if it is of limited magnitude, may be approximated piecewise to sections of constant velocity. The image distortion is evident as a variable along-track scale factor.

The effects of the aircraft motions discussed above are summarised in Fig 5.

4 AUTOFOCUSSING

Autofocus means that, in the absence of complete knowledge of flight path and scatterer geometry, the matched filter for processing is estimated from the raw data itself. This memorandum investigates three methods of autofocus: power spectra estimation, contrast optimisation, and multi-look image registration, and these are dealt with separately in subsequent sections. However, the need for autofocus is independent of which method is used, as is the inherent precision of the three methods. This section is concerned with the need for and precision of autofocus methods in general.

Autofocus is necessary if the aircraft deviates significantly from uniform straight line motion. The purpose of this section is to quantify what constitutes significant deviation from uniform straight line motion. A simple criterion is used to assess the significance of aircraft motion. It is assumed that a total phase error across the synthetic aperture in excess of π radians will degrade image quality. Whatever autofocus method is used it should not be expected to give results more accurate than the above phase error criterion suggests.

4.1 Depth of Velocity

The previous section discussed qualitatively the effects of various aircraft motions. Along-track velocity error and across-track acceleration both give rise to a signal history that is still a quadratic phase history and hence still a linear FM chirp. The only change is in the slope of the FM chirp. Consequently, any across-track acceleration can be expressed as a (range-dependent) effective along-track velocity error. This is done in most of this memorandum, and should be taken to mean an effective velocity error rather than an actual velocity error.

Depth of velocity means the velocity error that causes a total phase error across the aperture of π radians. Appendix 1 derives the depth of velocity in terms of the SAR system parameters. The depth of velocity is inversely proportional to the range and wavelength but more importantly it is proportional to the square of the resolution. Therefore, if resolution is improved by a factor of two, the tolerance to an along-track velocity error is reduced by a factor of four. An alternative and physically meaningful way of visualising the velocity error tolerance is to realise that only the relative velocity between the aircraft and scatterer is important. If the velocity error is interpreted instead as a scatterer moving along track, then the scatterer should not move so fast as to travel through more than a resolution cell during the illumination time.

The tolerance to across-track acceleration is derived in Appendix 2 and it is shown how to calibrate the across-track acceleration in terms of an equivalent range dependent velocity error. As with the velocity tolerance, the acceleration tolerance varies with the square of the resolution.

The aircraft motion represented by the depth of velocity should not be taken too rigorously since the criterion of π radians tolerable total phase error is open to discussion but it does represent a good estimate of the point where image deterioration starts to become a problem.

Fig 6 shows an example of the effects of velocity errors. The same raw data is shown after being processed at six different velocities. The image processed at the nominal aircraft velocity of 200 m/s is out of focus, demonstrating the need for autofocus. The optimum focus is seen to be at an effective velocity of 212.5 m/s. The remaining images indicate the sensitivity to velocity errors. A change of 2.5 m/s, which is of the order of two depths of velocity, produces obvious degradation of the image.

4.2 Depth of Along-track Acceleration

Along-track acceleration introduces a cubic term to the expected signal history. Appendix 3 derives the tolerance to across-track acceleration and shows that an acceleration can be tolerated that changes the velocity by four depths of velocity across a synthetic aperture. This shows that a limited effective along-track acceleration can be approximated by a piecewise approximation to a constant velocity without needing to include the cubic term in the matched filter. On the basis of typical velocity-azimuth plots, such an assumption is valid for the RSRE SAR system.

4.3 Autofocus Intervals

The autofocus estimate needs updating at intervals along track. This interval depends on two factors: the rate of change of focussing parameters, and the length of the synthetic aperture. These may be conflicting considerations. The raw data used to estimate the autofocus must necessarily average in some sense the aircarft motions occurring during that interval, and no autofocus method will be capable of resolving unknown motions with a structuremuch finer than the length of the raw data.

The length of raw data used for autofocussing is the sum of the synthetic aperture length and the width of the azimuth strip that is autofocussed. A minimum width of azimuth strip is required both for estimating the along track contrast and the registration of multilook images. This minimum width in addition to the synthetic aperture imposes a maximum rate of change that may be followed by the autofocus method.

Obviously, the higher the resolution of the processing, the tolerance to changes in aircraft motion reduces while the effect of averaging of motion changes due to longer synthetic aperture increases. Fortunately, the RSRE SAR system is just able to cope with the observed motion changes at the finer resolution, but in general this must be assessed for each SAR system in turn.

5 POWER SPECTRUM METHODS

This section describes a method of autofocus based on measurement of the power spectrum of the received signal. The principle on which the method is based is described, and then problems involved with its use are discussed.

In Fig 2, the received signal for a single scatterer passing through the beam is derived. The processing necessary to produce a SAR image consists of convolving the raw data with a matched filter, which is the complex conjugate of the single target response. Thus, if we could derive the single target response from the raw data, the matched filter could be simply constructed, without knowledge of the aircraft motion. To obtain the impulse response, it is necessary to identify an isolated strong point scatterer in the image, and extract the corresponding raw data.

Unfortunately, as will become apparent, we require updates to the matched filter approximately every 100 metres, and we cannot rely on isolated single scatterers being available throughout the length of the flight. Also, it is difficult to locate such scatterers; examination of a processed image is not reliable, since that image may itself be out of focus.

However, there is an alternative way to estimate the single target response, h. The received signal, r, is the convolution of the ground scatterer strength, s, with h:

$$r = s * h$$

Taking the Fourier transform of this equation gives the spectrum of the received signal for this range gate:

$$R = S.H$$

Now, if we average the power spectra for many range gates, we obtain

$$\langle |R|^2 \rangle = \langle |S|^2 \rangle . |H|^2 ,$$

since H is constant through many range gates. If the ground scatterer strength can be modelled as a Gaussian white noise process, $\langle |S|^2 \rangle = 1$, and thus $|H|^2$ is equal to $\langle |R|^2 \rangle$.

Although we cannot obtain a direct estimate of h from this process, since the phase of H has been lost, we can measure the width of $|H|$, and thus estimate the chirp rate, and so generate the required matched filter.

We can estimate the accuracy with which we can estimate H as follows: for a single spectrum, each point has a standard deviation equal to its mean, if we model the ground scatterer strength as Gaussian white noise. If we sum N range gates, the standard deviation is reduced by a factor $\sqrt{N}$. Thus, if for example we sum 100 power spectra, each sample of the power spectrum sum will have a standard deviation of 10% of its true value.

Fig 7 shows two power spectra sums, each obtained by summing 1500 range gates, which imples a standard deviation on each sample of approximately 2.5%. These graphs were obtained from raw data samples taken the same distance down track for each power spectrum sum, the difference between the two graphs being that the first was obtained for range gates in the near half swath, while for the second, range gates from the far half swath were used.

The two graphs should be identical in shape, apart from random variations whose amplitude was estimated above. However, it is clear that there are significant differences between the graphs. In particular, the graph for the second half swath is biassed towards negative frequencies. The reason for this is that the ground scatterer strength is not adequately modelled by a white noise process. In the second half swath, there is significantly more "scatterer strength" in the aft part of the beam than in the forward part.

This effect renders the power spectrum method described above useless; an attempt was made to select range gates that contained no strong scatterers, but for images of typical terrains, so few range gates may be usable that the summed power spectrum is too noisy to be used. Also, even if we can eliminate range gates containing strong scatterers, there may still be errors caused by variations in the scatterer strength on a longer scale (e.g a field may give a strong return because of terrain relief). Fig 8 shows the summed power in a processed image over 3000 range gates as a function of distance down track. The approximate length of the antenna illumination pattern is also shown. It is clear that there are significant variations in the mean scatterer power within this length.

In conclusion, although the mean power spectrum of a signal obtained as a result of a white noise input has been used in many applications to estimate point spread functions, this approach cannot be used here, because of the "non-white" characteristics of the ground scatterer strength. A model of ground clutter accounting for this non-white property has been proposed recently [4].

6 CONTRAST OPTIMISATION

Section 4 discussed autofocussing in general terms without any regard to a particular algorithm. This section is concerned with a particular algorithm based on contrast optimisation. Contrast optimisation is in principle a simple trial and error method of autofocussing. The trial consists of processing the raw data at a number of different effective velocities, and the particular processing velocity that produces the image with the maximum contrast is taken as the optimum effective velocity.

The whole method rests on the assumption that the maximum contrast image corresponds to the correctly focussed image. Such an assumption is intuitively reasonable but is not entirely foolproof. If the image consists of single isolated scatterers then the maximum contrast occurs when the modulus of the processed image of the scatterer attains a maximum, and that is obtained only when the scatterer is correctly focussed. However, real SAR imagery does not consist of isolated point scatterers. A very common feature of the imagery are fields that display a speckled image, although nominally the radar cross-section of the field is constant. This is the very opposite of the ideal isolated scatterer and cannot be used for focussing. Instead, areas in the image of high structural content should be used. These are likely to consist of strong scatterers but they are most unlikely to be isolated and the maximum contrast image is not necessarily the optimum focus, due to interference effects between the scatterers. However, on the average there is no reason to suppose that the interference

effects should display any asymmetry, and it is tacitly assumed that the averaging process is sufficiently efficient to reduce interference effects.

Autofocussing is computed at fixed intervals along track, the distance being a sensible compromise between spanning an excessive velocity change and having sufficient azimuth data to compute the contrast, as discussed in the general section on autofocussing. Contrast is defined as the standard deviation ofthe processed image pixels, normalised by dividing by the mean of the image pixels. This is done individually for each range gate and then averaged over all the range gates. Obviously, it is not practical to process all the range gates at all trial velocities. Therefore, an initial processing of all ranges at some estimated velocity is used to select a number of ranges for subsequent processing at the remaining trial velocities. The ranges are selected on the basis of maximum contrast, which favours rangegates of high structural content and discriminates against speckle.

The basic algorithm as described is summarised in a stylised language below:

```
FOR each step along track
      FOR each range gate
            process at estimated velocity
      NEXT range gate
      select maximum contrast range gates
      find maximum contrast velocity of selected range gates
      process all range gates at estimated velocity
NEXT step along track
```

The next three sections deal in more detail with the implementation of the algorithm.

6.1 Contrast Velocity Peak Detection

This section is concerned with a specific subsection of the stylised algorithm, namely:

find maximum contrast velocity of selected range gates

In order to select the maximum contrast velocity, the selected range gates need to be processed at different velocities. Clearly, it is not practical to process the range gates at all conceivable velocities. A compromise is necessary between effective averaging over many range gates and the time saved by focussing on fewer range gates. Empirically, 8 range gates were found to be too few and 16 range gates were found to be sufficient for reliable autofocussing.

The maximum contrast velocity is found in stages using a hierarchical algorithm. At each stage, three equi-spaced velocities are considered. The velocity spacing is specified in terms of the depth of velocity. This ensures that the spacing is scaled automatically to the SAR parameters, and in particular to the resolution of the SAR processing.Initially, the centre velocity is the best estimate of the processing velocity, which is usually the optimum velocity determined for the previous azimuth strip.

Having determined the triple of velocities, the selected range gates are then processed at these velocities. If the centre velocity possesses the highest contrast of the three velocities, control passes to the next stage of the maximum contrast algorithm. If not, the centre velocity is set equal to the maximum contrast velocity. In other words, there is a

step in the direction of increasing contrast, and this may be to a greater or smaller velocity, depending on which velocity possesses the highest contrast. This is repeated as many times as is necessary. Clearly, if a finite contrast function possesses at least one local peak, the algorithm will terminate in a finite number of steps.

At this stage, the estimate of maximum contrast is improved by interpolation. The interpolation fits a (unique) parabola to the three contrast velocity coordinates, and determine the maximum contrast velocity of the interpolated parabala. There is no theoretical justification for a parabolic interpolation, except that it is the lowest order expansion about the peak.

The maximum contrast algorithm is hierarchical because the same procedure can be repeated for three velocities with a smaller spacing, whose centre velocity is the interpolated velocity found from the previous velocity spacing. Typically, two or three levels are used, with spacings of, say, five, two, and one depths of velocity.

The maximum contrast velocity algorithm is demonstrated diagrammatically in Fig 9, and is given below in a stylised language:

```
set centre velocity to estimated velocity
FOR each velocity spacing
        generate triple of velocity coordinates
        compute contrast at each velocity
        WHILE centre velocity not the greatest contrast
                set centre velocity to maximum contrast velocity
                generate triple of velocity coordinates
                compute contrast at each velocity
        END WHILE centre velocity not the greatest contrast
        fit a quadratic to the contrast velocity coordinates
        set centre velocity to maximum contrast velocity of
                                interpolated parabola
NEXT velocity spacing
set estimated velocity to current centre velocity
```

The peak finding algorithm is very simple, and is well able to deal with any contrast velocity curves found in practice. Such a simple peak finding algorithm is effective because the general characteristics of the contrast velocity function are predictable. The function is typically dominated by a large peak whose width is of the order of a depth of velocity, although the main peak may exhibit subsidiary peaks of similar width on its flanks. Subsidiary peaks are eliminated from consideration by the hierarchical structure of the algorithm. Initially, the contrast velocity function is explored by samples more widely spaced than typical peak widths and, with an initial velocity spacing of four depths of velocity, say, the resulting interpolated maximum is inevitably in the region of the dominant peak. The sampling of the function at a reduced velocity spacing can then determine the location of the peak more precisely, with no fear of locking on to a subsidiary peak.

In summary, the performance of the peak detection algorithm has proved to be effective, efficient, and robust in its operation.

6.2 Velocity Hysteresis and Follow-Down Processing

Velocity hysteresis proved to be a problem when large changes of velocity occured between successive azimuth strips. The maximum contrast velocity tended to remain at the previous velocity estimate rather

than change to the new and significantly different velocity. The problem was easily detected by executing a forward and backward 'flight'. This is done by autofocussing azimuth strips in one order, and then using the same package to autofocus the azimuth strips in reverse order. Obviously, the autofocus results should be independent of the flight direction.

The maximum contrast velocity of a particular azimuth strip is used as the initial estimate of the maximum contrast velocity of the succeeding azimuth strip. At a large change in velocity, the initial estimate of velocity depends on the flight direction. This provides the channel by which the information on the previous velocity estimate is communicated, but it is not the root cause of the problem, because some initial estimate is always needed, whatever strategy is used to generate it.

The basic cause of the velocity hysteresis is the short-cut taken by processing a selected number of range gates that were selected on the basis of highest contrast. But the range gates are selected by initially processing the whole image at the initial velocity estimate that may be considerably different from the best focussing velocity. The reason for extracting those ranges of maximum contrast is to ensure a high structural content. However, if the initial processing is so much in error, then the whole image is badly blurred and any structural content tends to be lost. As a result, high contrast is no longer a reliable indicator of structural content. Instead, the range gates selected from the badly blurred image are those ranges whose interference effects of scatterers just happen to conspire to give a higher contrast at the initial processing velocity. It is also unlikely that the interference effects would conspire to give a maximum at all at the correct velocity. As a result, typical contrast velocity curves in these instances show a maximum at the initial velocity estimate that leads to the autofocus estimate 'getting stuck in a groove'. None of the hysteresis effect is due to the peak finding algorithm described in the previous algorithm, since the algorithm correctly located the erroneous peaks.

The solution adopted is called follow-down processing. If the velocity change is too large in terms of the depth of velocity, then the velocity change itself cannot be reduced but the depth of velocity can be increased by processing at a coarser resolution. By processing at the coarser resolution, the image structural content is preserved, and although the number of independent measurements of structure is reduced by the coarser resolution, it can nevertheless distinguish between speckle and regions of relatively few scatterers. Alternatively, the reduced resolution processing may be regarded as detuning the matched filter by using only that length of raw data that may be matched adequately by the initial erroneous filter. The processing is then prevented from choosing those range gates that happen to be 'tuned' to the longer high resolution filter. As a result of processing at the lower resolution, no account can be taken of the interference effects of raw data and the extremes of the longer filter, (a form of randomised additive noise),and hence the bias of the selected range gates towards the initial velocity estimate is eliminated.

The follow-down processing involves processing the whole image at the reduced resolution to select the range gates for contrast maximisation. The maximum contrast velocity is then determined using the peak detection algorithm that also processes the gates at reduced resolution. The follow-down processing continues by repeating the peak detection algorithm at a finer resolution by using the coarse resolution maximum contrast velocity as the initial velocity estimate. This process can be repeated through finer

and finer resolution until the desired resolution is obtained. In practice it is found that the follow-down processing works well if a resolution four times poorer is used for the initial follow down processing. Only one or two steps are needed to reach the required resolution.Appendix 3 suggests a reasonable starting resolution for follow-down processing, if an estimate of maximum velocity changes is known a priori.

The follow down processing is presented in a stylised language below.

```
FOR each range gate
        process each range gate at reduced resolution
NEXT range gate
select maximum contrast range gates
FOR each finer resolution
        find maximum contrast velocity of selected range gates
NEXT finer resolution
```

The follow-down processing is remarkably effective in removing the effects of velocity hysterisis. The effectiveness of the method is illustrated in Figs 10 and 11. Fig 10 shows four contrast velocity curves derived by processing at the finest resolution at four different initial velocity estimates from 200 to 230 metres/second. The two curves at 200 and 230 m/s display a false maximum at the initial estimate velocity used to select the range gates. The depth of velocity is of order 1 m/s and, since the true effective velocity is 215 m/s, this represents an error in the initial estimate of 15 depths of velocity. If the range gates are selected by processing at a resolution four times poorer, the resulting contrast curves at the required resolution in Fig 11 show excellent agreement with no subsidiary peaks and the main peak correctly located.

This completes the description of the maximum contrast algorithm which is presented as a whole in Appendix 5.

6.3 Results

The effectiveness of follow-down processing in eliminating velocity hysteresis is shown in Fig 12, which shows the estimated effective velocity for a forwards and a backwards flight processed at the finest resolution. The two curves agree well within the expected error of order of the two-sided depth of velocity of 2 m/s. This demonstrates the effectiveness of autofocus by contrast maximisation, which can be recommended as a viable method for autofocus within the limitations imposed by the depth of velocity.

It is surprising that the autofocus method is able to cope with the larger changes in effective velocity because within the azimuth strip used for autofocus there may be up to 10 depths of velocity change in velocity. Clearly, if the range gates selected for focussing contained bright targets to one side of the azimuth strip, this would bias the velocity estimate to the velocity on that side of the strip. However, if we assume that each range contains one small region of high structural content, and the location of these regions is independent in each range gate, then the distribution of the centroid of 16 such regions should have a mean at the strip centre and a standard deviation of order of one quarter of a strip width. This is slightly pessimistic to assume that each range gate contains only one region of high contrast. This would seem to explain the ability of autofocus to cope with such large velocity changes.

The consistency of autofocus in regions of high velocity changes does not alter the fact that, if the strip is processed at the estimated autofocus velocity, the edges of the strip will be out of focus. A modified processing program was developed to divide an azimuth strip into substrips that limited the velocity change across a substrip to a depth of velocity, but curiously, the resulting processed image did not appear to be improved, either by eye, or by measuring the contrast of the processed image. It is not really understood why no improvement was observed, especially since it is a more generous tolerance than the Rayleigh quarter wave limit that allows a total phase error of only $\pi/2$. Nevertheless, it appears to suggest that for visual interpretation of the image the criterion for adequate focus may in fact be relaxed somewhat.

7 Focussing by Multilook Registration

Section 6 described a method which estimated the optimum focussing parameters by maximising a particular property of the image, namely the contrast. This section describes a method which is based on measurement of the difference between two images of the same scene - multilook images. The generation of multilook images is described in [1]. Here we shall show how multilook imagery can be used to focus an image, and describe how the method is implemented. Results of the application of the method will then be given.

7.1 Theory

Multilook images can be obtained by processing different parts of the returned signal for a single scatterer independently. For example, two look images can be derived from the positive and negative frequency components in the raw signal independently. More than two looks can be obtained by partitioning the raw signal spectrum appropriately. For a perfectly focussed image, the looks overlay each other exactly, and can, if required, be summed incoherently to provide a degree of speckle reduction. However, as will be shown below, if the images are not correctly focussed, the images are displaced with respect to each other in the azimuth direction. This means that the images cannot be summed to perform speckle reduction without degrading the resolution (unless the misregistration is first corrected). However, this misregistration can also be used as a focussing method: the focussing parameter is varied until the multilook images are in registration. The implementation of this method will be described below; first we estimate the accuracy of the velocity estimate we can expect to obtain using this method.

Consider a system in which two looks are generated: one each from the positive and negative frequency components of the received signal. For a resolution σ in a single look system, the synthetic aperture length is LSA. If we require two looks, to keep the synthetic aperture length constant, the resolution in each look will be doubled. For a synthetic aperture length LSA, the time between the two looks is given by

$$\Delta T = LSA/2v$$

If the velocity of the aircraft is known accurately, then the two looks misregister by a known amount which can be corrected. However if the velocity is in error by Δv, then there will be a further, uncorrected, shift between them, equal to $\Delta v\ \Delta T$.

If the velocity is in error by one depth of velocity, then the misregistration between the two looks is

$$\Delta x = \Delta v \ \Delta t = \frac{\sigma v}{LSA} \cdot \frac{LSA}{2v} = \frac{\sigma}{2}$$

Thus, the two looks misregister by one half of the resolution cell size when the velocity is in error by one depth of velocity. This shows that this method of autofocus can estimate the best processing velocity to approximately the same degree of accuracy as the contrast maximisation method, provided we can obtain a sufficiently accurate estimate of the misregistration. Note also the misregistration depends on the degree of velocity mismatch, and that when there is no velocity error, $\Delta v = 0$, the two looks register exactly ($\Delta x = 0$).

7.2 Implementation

We have shown that measurement of the misregistration of two images obtained from the positive and negative frequency components of the raw signal can be used to estimate the best processing velocity. This section describes the way in which the misregistration is measured and the velocity estimate obtained.

Cross-correlation of two misregistered images is the standard way of estimating the shift between them. For two dimensional images, f and g, the correlation surface h is defined by

$$h_{k\ell} = \sum_i \sum_j f_{ij} \, g_{i+k, \ell+j}$$

In this case, we are only interested in misregistration in the azimuth direction, and thus we can obtain a cross correlation line for each range gate independently:

$$C_k = \sum_i i1_i \, i2_{i+k}$$

where i1,2 are the two looks obtained for a particular range gate. The position of the peak in the cross-correlation line gives the misregistration between the two images.

For incoherent images, with low noise levels, cross-correlation is an extremely reliable method for measuring the misregistration between two images. However, due to the speckle in SAR Images, the images of a single range gate may not register correctly (e.g if there are no very strong scatterers in this range gate, the peaks in the speckle noise will be aligned as well as possible). Therefore, the cross correlation functions for many range gates are summed, in order to suppress the effects of speckle noise.

Even when a large number of range gates' correlation lines have been summed, the peak position for a single processing velocity may still not be a reliable indicator of the misregistration between the looks, and hence may not be suitable as a measure of the error in the processing velocity. This problem is overcome by processing each range gate with a number of different velocities: in Appendix 4 we show that the misregistration between the two looks is given by

$$\Delta x \ \alpha \left(\frac{v^2}{v_p^2} - 1 \right)$$

where v_p is the processing velocity used, and v the true velocity. Thus a straight line fit of the misregistration against the inverse processing velocity squared has intercept (zero misregistration) at a velocity corresponding to the best processing velocity. The straight line fit also gives a measure of the accuracy of the velocity estimate.

Range gates are processed, and their correlation lines summed, until the accuracy of the velocity estimate reaches a user-defined level. For each strip, five velocities are used: the velocity estimate from the previous strip, and plus and minus one and two depths of velocity.

7.3 Results

This algorithm was run to obtain velocity estimates for forward and backward runs over the same data as the contrast maximisation method. As for that method, in regions where the velocity was changiang rapidly, very poor velocity estimates were sometimes obtained. For the contrast maximisation method, this problem arises because of range gate selection, which can bias the velocity estimate towards that obtained for the previous strip, unless follow down processing is used. For the misregistration method there is no biassing, but if the velocity is changing rapidly, all five processing velocities may lie far from the true velocity. Then all the multilook images are badly out of focus, leading to a high uncertainty in the correlation peak position for each velocity, and hence a low accuracy velocity estimate.

In order to correct for possible errors due to this effect, two passes are performed for each strip. The aim of the first pass is to obtain an approximate velocity estimate and the velocities for the second pass are centred around the velocity estimate obtained for pass one. When pass two has converged to a sufficiently accurate velocity estimate, it is recorded, and the program moves on to the next strip. In order to eliminate problems in regions where the velocity is changing rapidly, the first pass is done at lower resolution than that required for the final velocity estimate. Due to the greater depth of velocity at lower resolution, the five velocities used are more widely spread, which means that some of the multilook images are more likely to be better focussed, and hence give better correlation surfaces. A further advantage to performing the first pass at lower resolution is that shorter reference functions are required, with consequently shorter processing time. The velocity estimation algorithm is expressed in a stylised language in Appendix 5.

Graphs of effective velocity against azimuth position are shown in Fig 13, for a forwards and backwards run, using the same raw data and synthetic aperture length as those used to generate Fig 12 via the contrast maximisation method. (It must be remembered that to obtain a resolution σ for two looks requires the same synthetic aperturelength as that for resolution $\sigma/2$, single look.) It is clear that the performance of the algorithm is as good as the contrast method. Comparison of the two methods is deferred to Section 8.

8 SUMMARY

The velocity curves of Figs 12 and 13 indicate regions of high velocity change between azimuth strips. If these were actual velocity changes, it would imply aircraft acceleration of up to 2 g along track. Alternatively, the same effect would be achieved with across track accelerations of order of up to 0.03g. These figures do suggest that the aircraft motion error is predominantly across track.

The algorithms used to autofocus assume along-track velocity errors rather than across-track acceleration. Assuming that the motion is predominantly across-track, there should be some discernible difference in range dependence if the range swath were a large fraction of the actual range. In order to check for a range dependency, the range swath was divided into two halves: near and far. The velocity plots for the two half swaths for both contrast and misregistration methods are shown in Figs 14 and 15. In each case, the near and far swath velocities agree within 2 metres/sec which is the two-sided depth of velocity. Typical range swaths are of order 10% of the actual range, which implies a change in the effective velocity of order 5%. However, an average range separation is likely to be half the maximum possible range difference, giving an average velocity discrepancy between half swaths of order 2.5%. A modified version of the autofocus algorithms for the contrast and misregistration methods, which assumed along-track acceleration, was used to check for any improved agreement between half swaths, but no improvement was observed. This is a little surprising since the two-sided depth of velocity tolerance of 1% suggests that a difference should be just noticeable. Since in practice no difference could be discerned between the two motion errors, the parameterisation in terms of effective along-track velocity is acceptable.

The most important conclusion to be drawn from the agreement between the two half swaths is that, in the absence of any knowledge of the actual motion parameters, it provides a check on the self consistency of the autofocus methods. It can be seen that both contrast and misregistration methods succeed in autofocussing the data to within the required tolerance.

9 CONCLUSIONS

Three methods of SAR autofocus have been discussed. The method based on power spectrum was found to be unreliable. The other two remaining methods based on contrast optimisation and misregistration can both be recommended for autofocus of SAR data.

REFERENCES

1 Kovaly J J, Synthetic Aperture Radar, Artech House, 1976.

2 Hovanessian S A, Introduction to Synthetic Array and Imaging Radars, Artech House, 1980.

3 Tomiyasu K, Review of Synthetic Aperture Radar, Proceedings of IEEE, Vol 66, May 1978, pp 563-583.

4 Oliver C J, Opt. Acta, Vol 31, pp 701-722 1984.

APPENDIX 1

RESOLUTION OF SYNTHETIC APERTURE RADAR

The following is a simple heuristic derivation of the resolution of a SAR system.

conventional resolution = $R.\theta$

;where R = range and θ = real beamwidth

The far field angular distribution of a radar antenna is the Fourier transform of the antenna aperture weighting. For a uniform antenna weighting, the beam profile is a sinc function of width:

$\theta = \lambda/l$

;where λ = radar wavelength
and l = antenna length

Therefore

conventional resolution = $R.\lambda/l$

Since we are assuming a synthesised antenna of length Lsa, and remembering that the SAR system depends on the two-way path differences, then

SAR resolution = $R.\lambda/2.Lsa$

This is only an approximate derivation and does not take into account the actual beam profile, especially since the effective single scatterer response is the square of the illumination profile, due to the two way propagation path. Since we have assumed rectangular illumination any loss of energy in the components of higher frequency reduces the effective bandwidth and must therefore lead, to some extent, to a poorer resolution.

APPENDIX 2

AIRCRAFT MOTION TOLERANCE

i) Depth of Velocity

Depth of velocity is defined as that velocity error that causes a total error of II radians across the synthetic aperture. The parabolic variation of the two-way distance of the scatterer was derived in Fig 2:

$2.dR = x^2/R$; x = distance from broadside

$2.dR = v^2.t^2/R$; v = aircraft velocity

; t = time from broadside

The phase error of π radians corresponds to a distance of $\lambda/2$, which implies an error of $\lambda/4$ at the edge of the beam. Therefore, from the definition of depth of velocity:

$$2(dR_{v+dv} - dR_v)\Big|_{t = Lsa/2v} = \frac{\lambda}{4}$$

$$\frac{[(v + dv)^2 - v^2]}{R} = \frac{Lsa}{4.v} = \frac{\lambda}{4}$$

$$\frac{dv.Lsa^2}{2.v.R} + \frac{dv^2.Lsa^2}{4.v^2.R} = \frac{\lambda}{4}$$

The second term may be neglected for small velocity change:

$$\frac{dv}{v} = \frac{R.\lambda}{2.Lsa} = \frac{\sigma}{Lsa} = \frac{2.\sigma^2}{R.L_{SA}} \quad ; \sigma = \text{resolution}$$

Rearranging as:

$$\frac{Lsa}{v} = \frac{\sigma}{dv}$$

This shows that the time takent to traverse the synthetic aperture is the same as the time taken to traverse a resolution cell at the depth of velocity.

The depth of velocity is so called in analogy to the term depth of field used for optical systems. However, depth of field is usually quoted as the total variation of range that maintains acceptable focus, but it should be noted that the depth of velocity derived is only the one-sided velocity tolerance.

ii) Depth of Across-track Acceleration

Assume a parabolic trajectory due to across-track acceleration of the aircraft.

$$2.dR = a.t^2$$

Depth of across-track acceleration is defined as that acceleration which causes a total phase error of II radians across the synthetic aperture:

$$2.dR\Big|_{t = Lsa/2v} = \frac{\lambda}{4}$$

$$a.\frac{Lsa^2}{4.v^2} = \frac{\lambda}{4}$$

Depth of across-track acceleration, $a = \frac{\lambda.v^2}{Lsa^2} = \frac{4.\sigma^2.v^2}{R^2.\lambda}$

iii) Velocity and Across-Track Acceleration Equivalence

The equivalence is found by equating the terms that give rise to phase errors of π radians.

$$\frac{dv}{v} \cdot \frac{Lsa^2}{2.R} = \frac{a}{v^2} \cdot \frac{Lsa^2}{4}$$

$$a = \frac{2.v.dv}{R} \quad \text{or,} \quad a = \frac{d(v^2)}{R}$$

iv) Depth of Along-Track Acceleration

In the presence of an acceleration term, the along-track position

$$x = (vt + ft^2/2) \qquad ; f = \text{along-track acceleration}$$

Equating the phase error at the edge of the beam to $\lambda/4$:

$$2.(dR_{v,f} - dR_{v,o}) = \frac{\lambda}{4}$$

$$\frac{v.f.t^3}{R} + \frac{f^2.t^4}{4.R} = \frac{\lambda}{4}$$

The final term may be neglected for small accelerations.

$$\frac{v.f}{R} \cdot \frac{Lsa^3}{8.v^3} = \frac{\lambda}{4}$$

Therefore

$$\text{Depth of along-track acceleration} = \frac{2.R.\lambda.v^2}{Lsa^3} = \frac{16.\sigma^3.v^2}{R^2.\lambda^2}$$

Unlike across-track acceleration, which affects the scatterer range directly, the range is perturbed by a second order effect. Consequently, we expect a relatively generous tolerance to along-track acceleration. As with the along-track velocity error, the physical cause may in fact be a changing across-track acceleration which may be interpreted as an effective along-track acceleration.

Rearranging the above expression:

$$f = 4.dv. \frac{v}{Lsa}$$

$$f = \frac{4.dv}{T} \quad ; T = \text{time to traverse a synthetic aperture}$$

This demonstrates that an effective along-track acceleration may be approximated linear piecewise if the effective acceleration does not change the effective velocity by more than four depths of velocity through a synthetic aperture.

APPENDIX 3

INITIAL RESOLUTION FOR FOLLOW-DOWN PROCESSING

The initial processing resolution should be chosen such that the change of velocity across the length of raw data used to process an azimuth strip is of order of a depth of velocity in order to avoid excessive defocussing at the edge of the strip.

Let the maximum spatial rate of change of velocity,

$$\frac{dv}{dx}_{max} = Vxm$$

where v is the aircraft velocity and x is the distance along track

Then equating the velocity change across a synthetic aperture with the depth of velocity:

$$dv = \frac{dv}{dx}_{max}.Lsa = \frac{Vxm.R.\lambda}{2.\sigma}$$

where Lsa is the synthetic aperture length, R is the range, λ is the wavelength, and σ is the resolution.

But the depth of velocity may be expressed in terms of the SAR parameters (Appendix II)

$$dv = \frac{2.v.\sigma^2}{R.\lambda}$$

Therefore

$$\frac{2.v.\sigma^2}{R.} = Vxm \cdot \frac{R.\lambda}{2.\sigma}$$

Rearranging in terms of the processing resolution:

$$= \sqrt[3]{\frac{R^2.\lambda^2.Vxm}{4.v}}$$

This then gives an indication of a suitable initial resolution for follow-down processing.

APPENDIX 4

DEPENDENCE OF MISREGISTRATION ON DEFOCUS

In this appendix we derive the misregistration between looks in a multilook processor, as a function of defocus. Refer to Fig 16. For a single scatterer passing through the beam, the Doppler frequency changes linearly with time:

$$f(t) = \beta t$$

where

$$\beta = \frac{4\pi v^2}{R_o \lambda}$$

The scatterer remains in the beam for a time 2T.

Now, suppose we process this frequency history to produce n looks, but using a processing parameter, β_p, corresponding to a velocity v_p. Consider, for example processing the two "end" looks. Then the part of the signal history labelled "A" will produce an image at time t_1 given by

$$t_1 = T(1 - \frac{1}{n}) \frac{(\beta - \beta_p)}{\beta_p}$$

Similarly, the part of the spectrum labelled "B" will produce an image at time

$$t_2 = - t_1$$

Note that this analysis assumes that there are no higher order terms in the frequency function.

Thus the misregistration, in time, between the two images is

$$\Delta t = 2T \left(1 - \frac{1}{n}\right)\left(\frac{\beta}{\beta_p} - 1\right)$$

For a two look system, and substituting for β and β_p, we obtain

$$\Delta t = T\left(\frac{v^2}{v_p^2} - 1\right)$$

APPENDIX 5

AUTOFOCUS ALGORITHMS

The autofocus algorithms are presented below:

A5.1 Contrast Optimisation Algorithm

```
FOR each step along-track

    FOR each range gate

        process at reduced resolution with estimated velocity

    NEXT range gate

    select maximum contrast range gates

    FOR each finer resolution

        set centre velocity to estimated velocity

        FOR each velocity spacing

            generate triple of velocity coordinates
            compute contrast at each velocity

            WHILE centre velocity not the greatest contrast

                set centre velocity to maximum contrast velocity
                generate triple of velocity coordinates
                compute contrast at each velocity

            END WHILE centre velocity not the greatest contrast

            fit a parabola to the contrast velocity coordinates
            set centre velocity to maximum contrast of interpolated parabola

        NEXT velocity spacing

        set estimated velocity to current centre velocity

    NEXT finer resolution

    process all range gates at estimated velocity

NEXT step along-track
```

A5.2 Misregistration Algorithm

```
FOR each autofocus strip

    FOR each pass

        set the resolution for this pass
        generate the processing velocities
        zero the correlation line sums

        WHILE velocity estimate is not sufficiently accurate

            select a new range gate at random

            FOR each processing velocity

                generate two looks
                cross-correlate the two looks
                add the correlation line to the correlation line sum
                find the peak of the correlation line sum

            NEXT processing velocity

            perform straight line fit of peak position against 1/vp squared
            find intercept and its uncertainty

        END WHILE velocity estimate is not sufficiently accurate

    NEXT pass

record estimated velocity for this autofocus strip
process all range gates at estimated velocity

NEXT autofocus strip
```

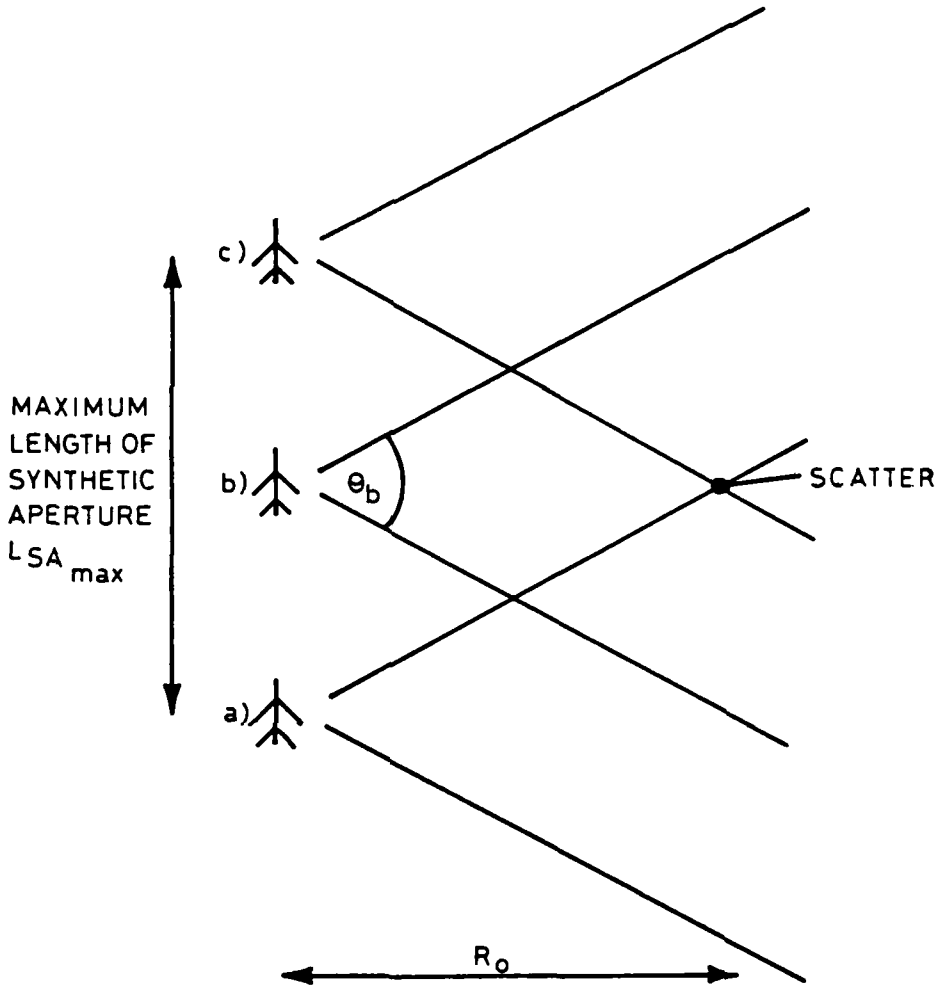

a) Scatterer entering beam

b) Scatterer broadside

c) Scatterer leaving beam

$$L_{SA_{max}} = R_o \, \theta_b$$

FIG. 1. LENGTH OF SYNTHETIC APERTURE

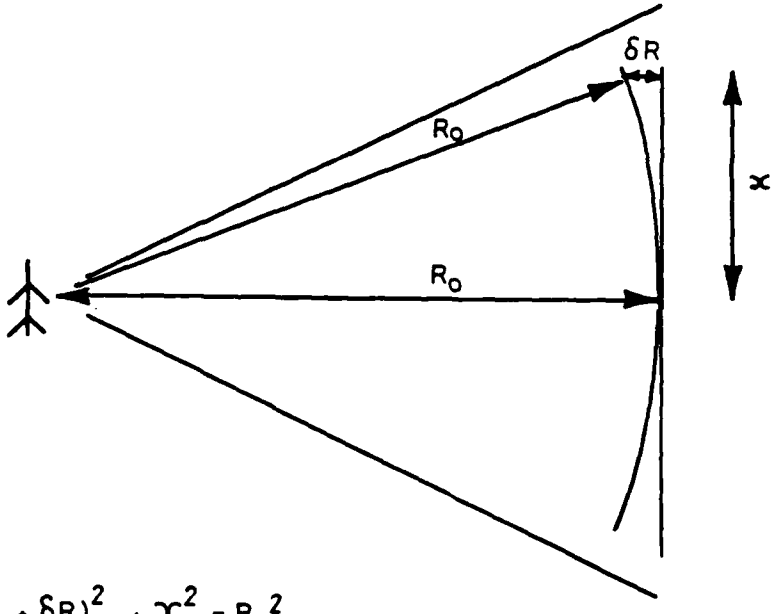

Pythagoras : $(R_o + \delta R)^2 + x^2 = R_o^2$

$$\therefore 2\delta R = \frac{x^2}{R_o} \quad \text{(small angle approximation)}$$

$$\therefore \text{phase } \phi = \frac{2\pi(2\delta R)}{\lambda} \quad \text{(two way path)}$$

$$\phi = \frac{2\pi x^2}{R_o \lambda}$$

Signal history may be expressed as the complex signal $\exp.(2\pi j x^2 / R_o \lambda)$

FIG. 2. SINGLE SCATTERER PHASE HISTORY

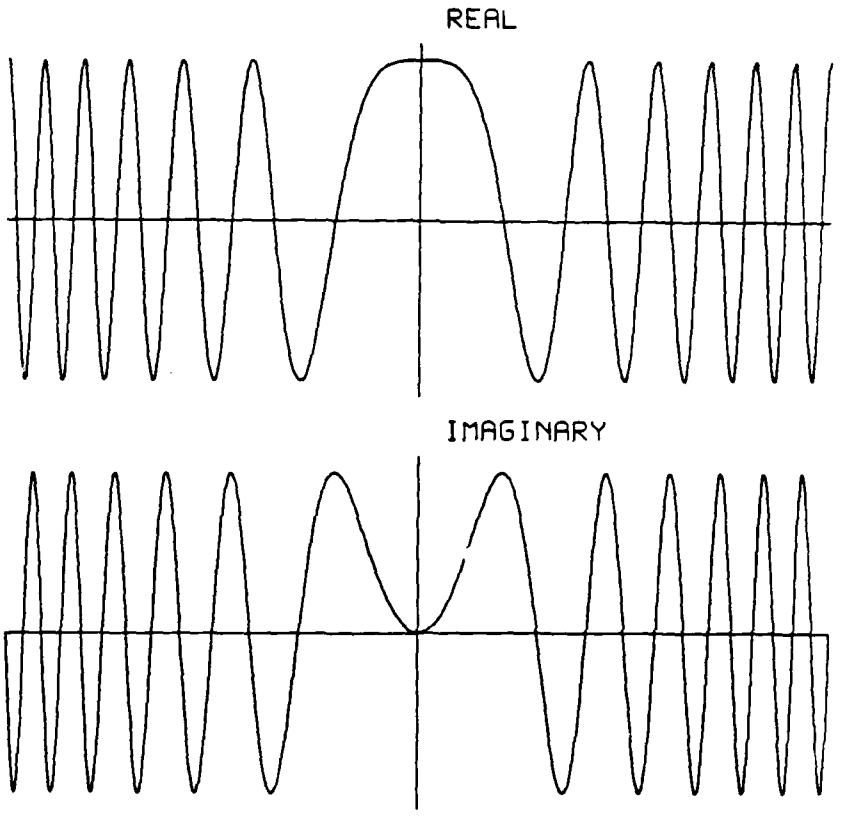

COMPLEX SIGNAL HISTORY $\exp (- j k x^2)$

COMPLEX REFERENCE FUNCTION $\exp (+ j k x^2)$

FIG 3 REAL AND IMAGINARY REFERENCE FUNCTIONS

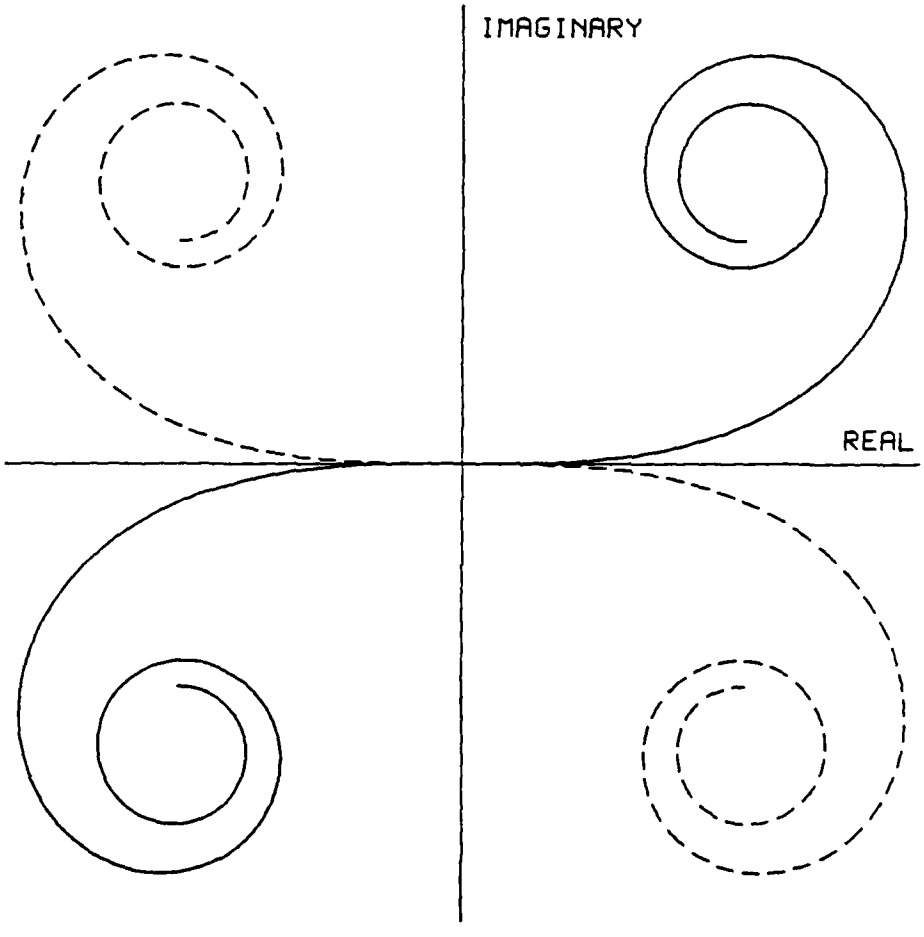

——————— SIGNAL PHASOR DIAGRAM

- - - - - - - - - - REFERENCE PHASOR DIAGRAM

FIG 4 SINGLE SCATTERER PHASE HISTORY

MOTION	DISTORTION	PROCESSING
ALONG-TRACK		
positional error	displaced image	
velocity error	along-track scale change	defocus
acceleration	variable scale change	variable defocus
ACROSS-TRACK		
positional error	displaced image	
velocity	rotation	
acceleration	variable rotation	defocus

FIGURE 5 EFFECTS OF AIRCRAFT MOTION

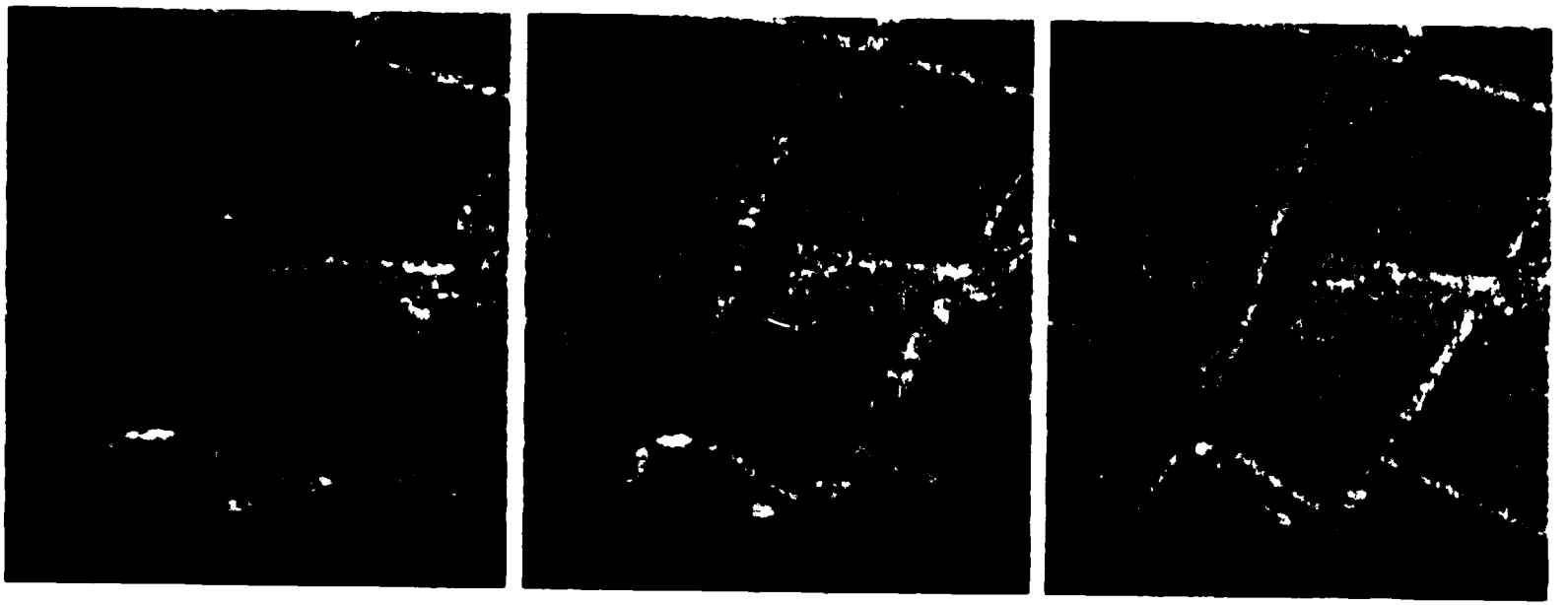

FIG 6 SAR IMAGE PROCESSED AT SIX VELOCITIES

(Continued Overleaf)

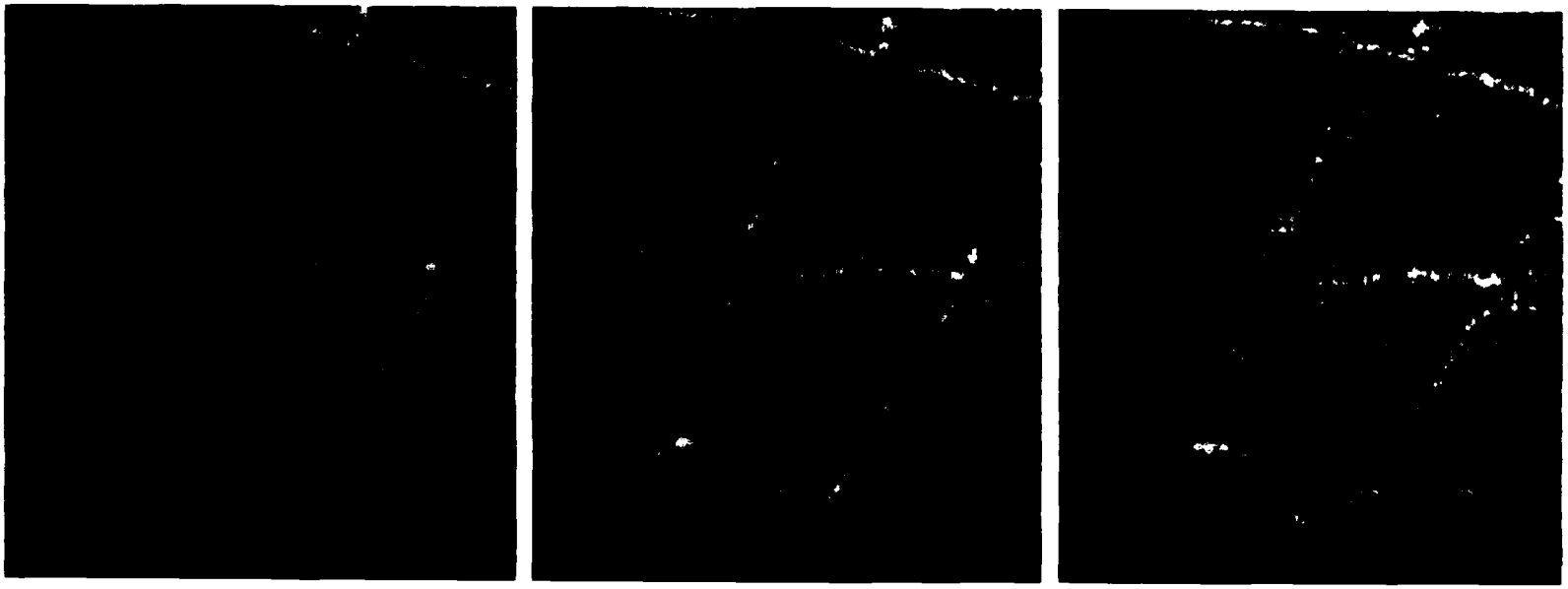

(Optimum Focus)

FIG 6 (Continued)

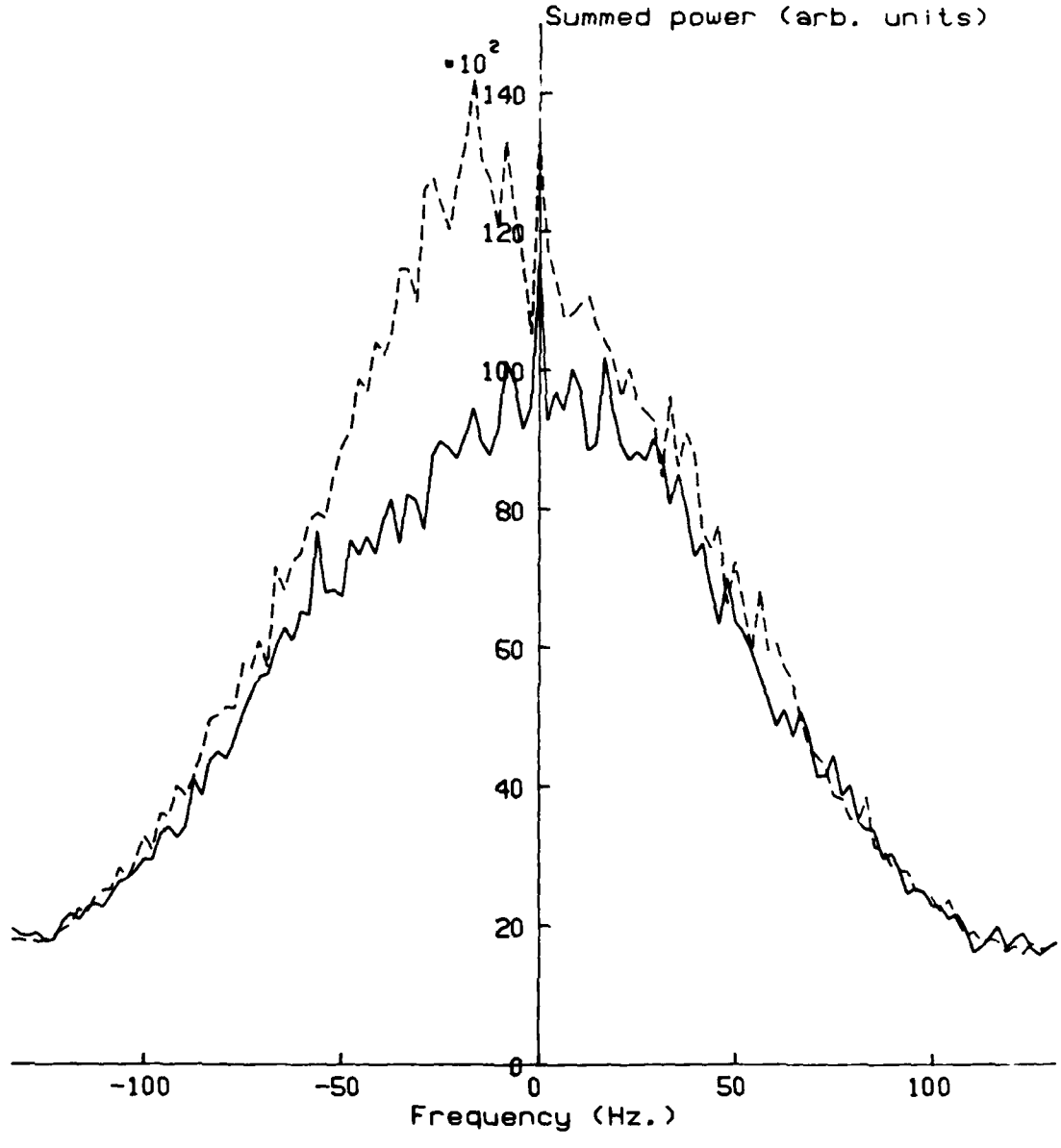

FIG.7 EXAMPLES OF SUMMED POWER SPECTRA

Summed over 1500 range gates

——— Near half swath

------ Far half swath

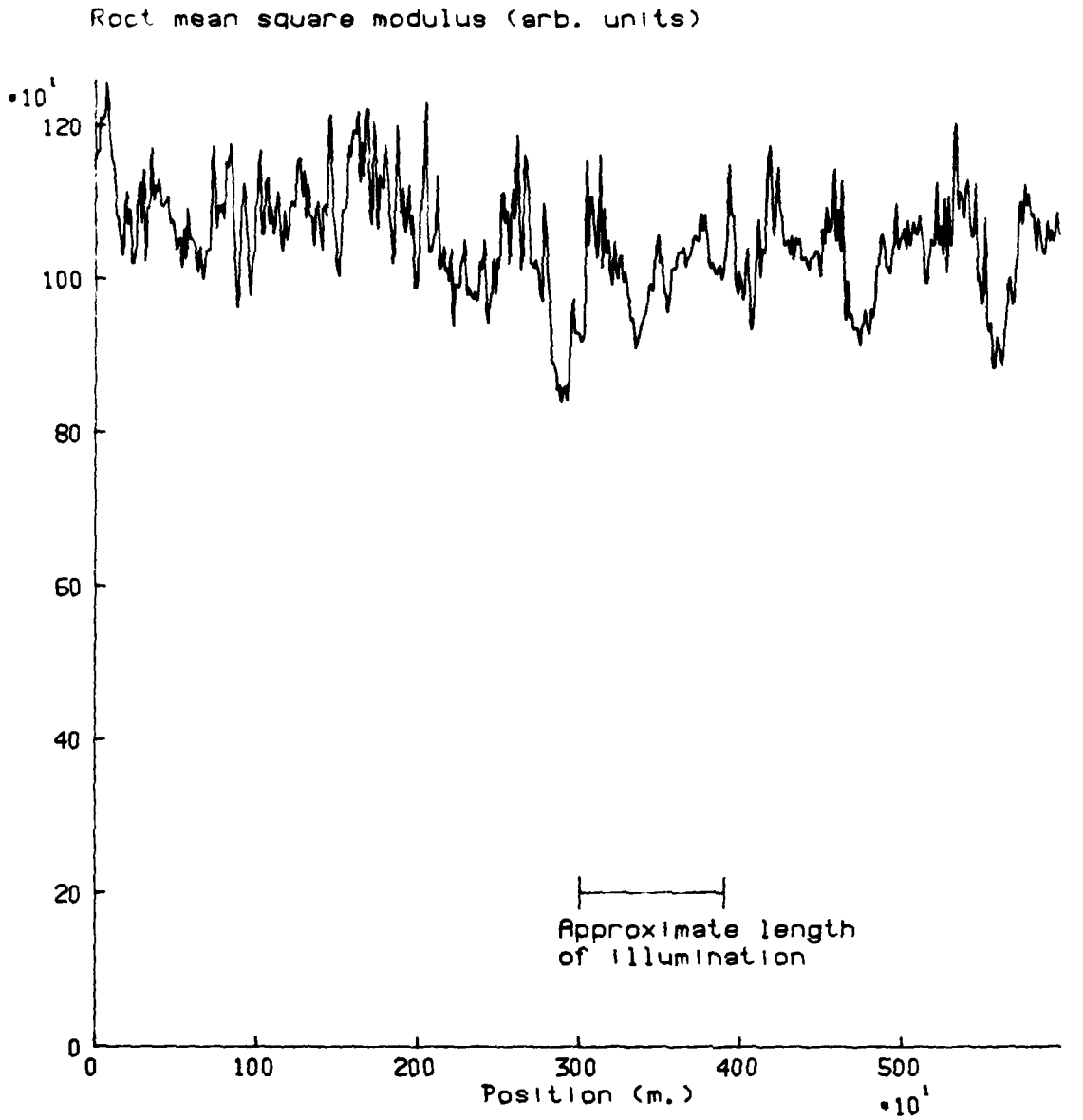

FIG.8 ROOT MEAN SQUARE MODULUS VALUES FOR A TYPICAL SAR DATA TAPE

Calculated over 3000 range gates

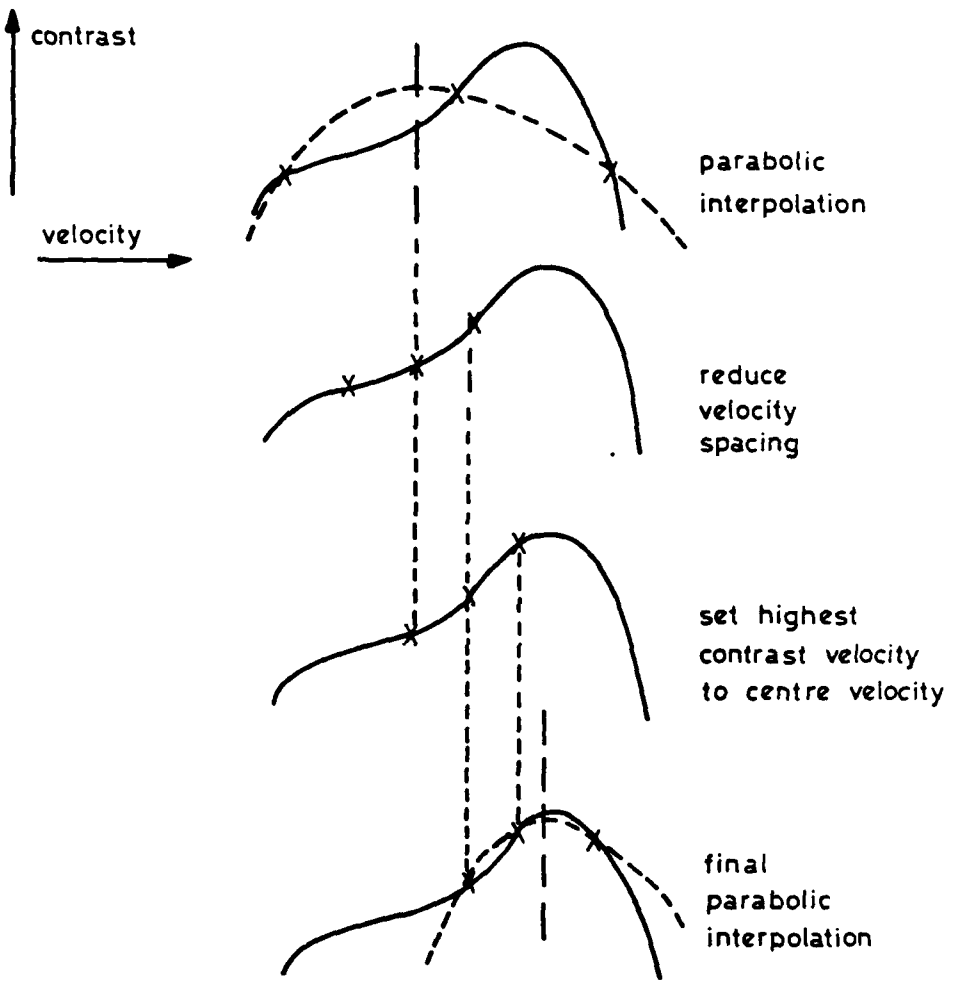

FIG.9. PEAK ESTIMATION ALGORITHM

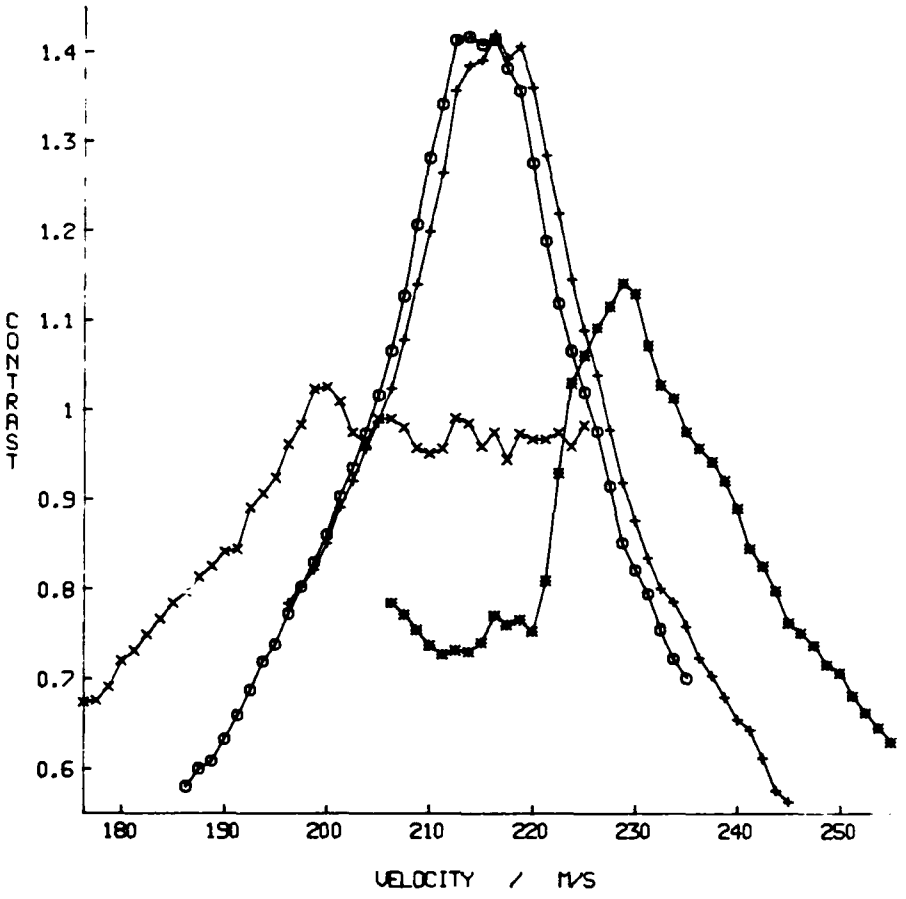

PROCESSING VELOCITY USED FOR RANGE GATE SELECTION:

X 200 m/s

0 210 m/s

+ 220 m/s

*** 230 m/s**

FIG 10 CONTRAST VELOCITY CURVES FOR RANGE GATES SELECTED AT FULL RESOLUTION

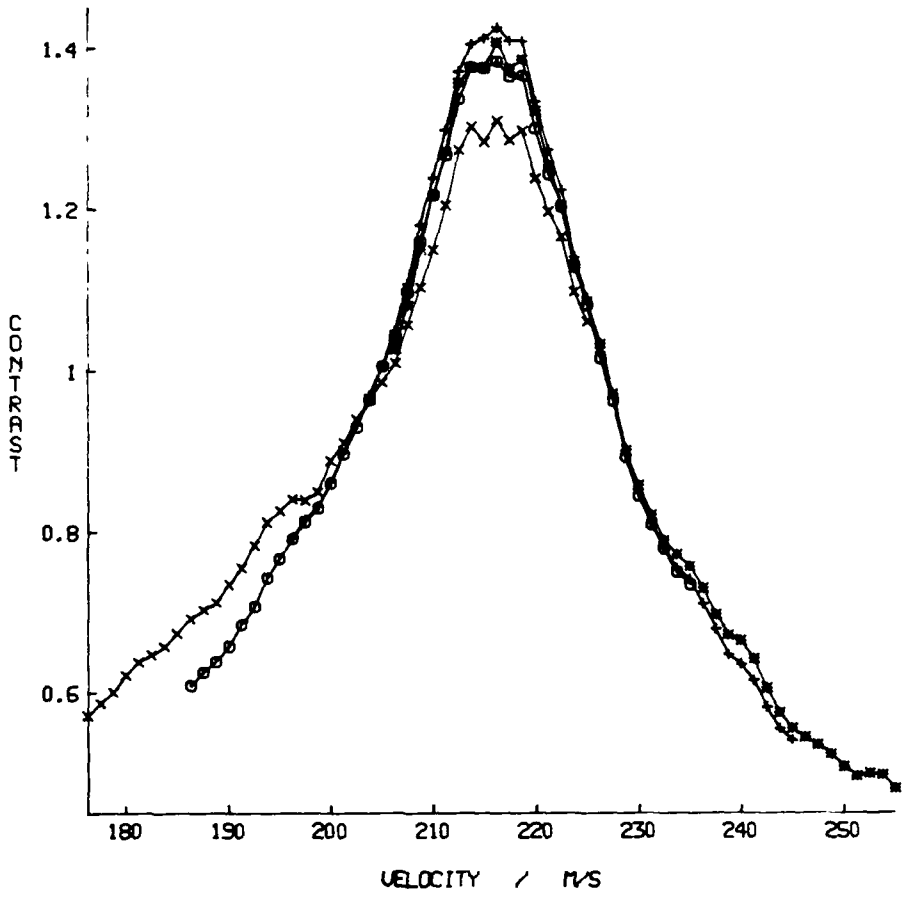

PROCESSING VELOCITY USED FOR RANGE GATE SELECTION:

X 200 m/s

0 210 m/s

+ 220 m/s

*** 230 m/s**

FIG 11 CONTRAST VELOCITY CURVES FOR RANGE GATES SELECTED AT REDUCED RESOLUTION

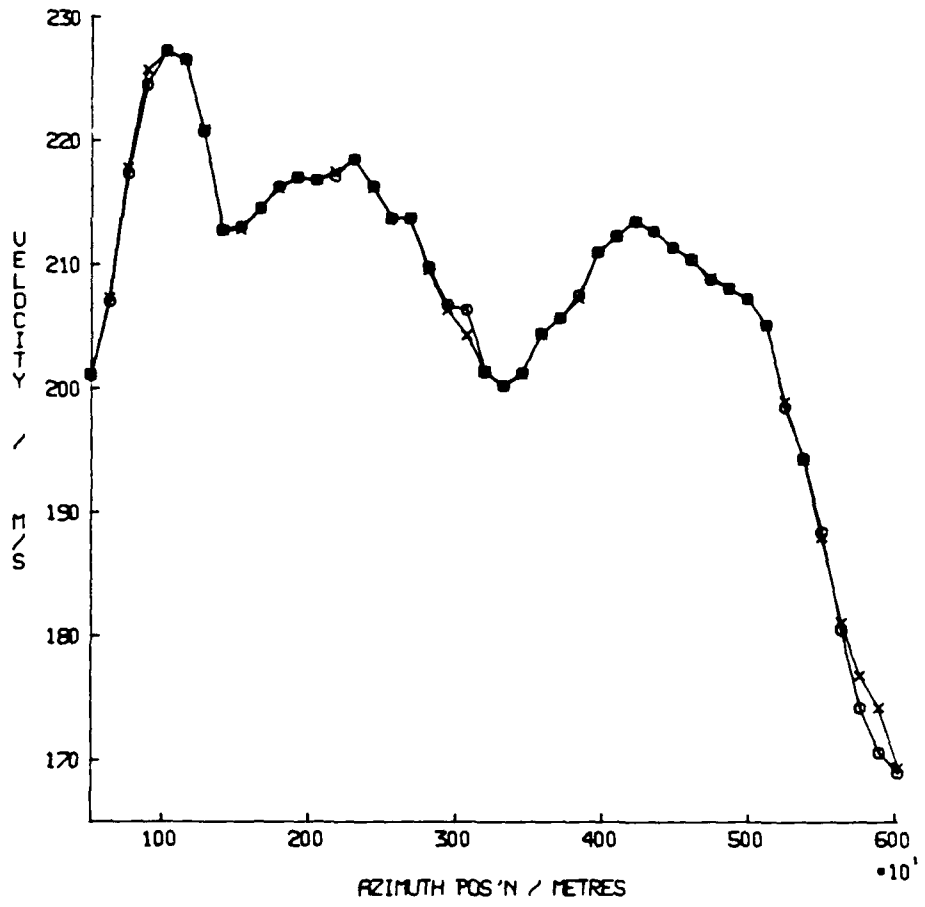

FIG 12 FORWARD AND BACKWARD VELOCITY PLOT USING CONTRAST OPTIMISED AUTOFOCUS

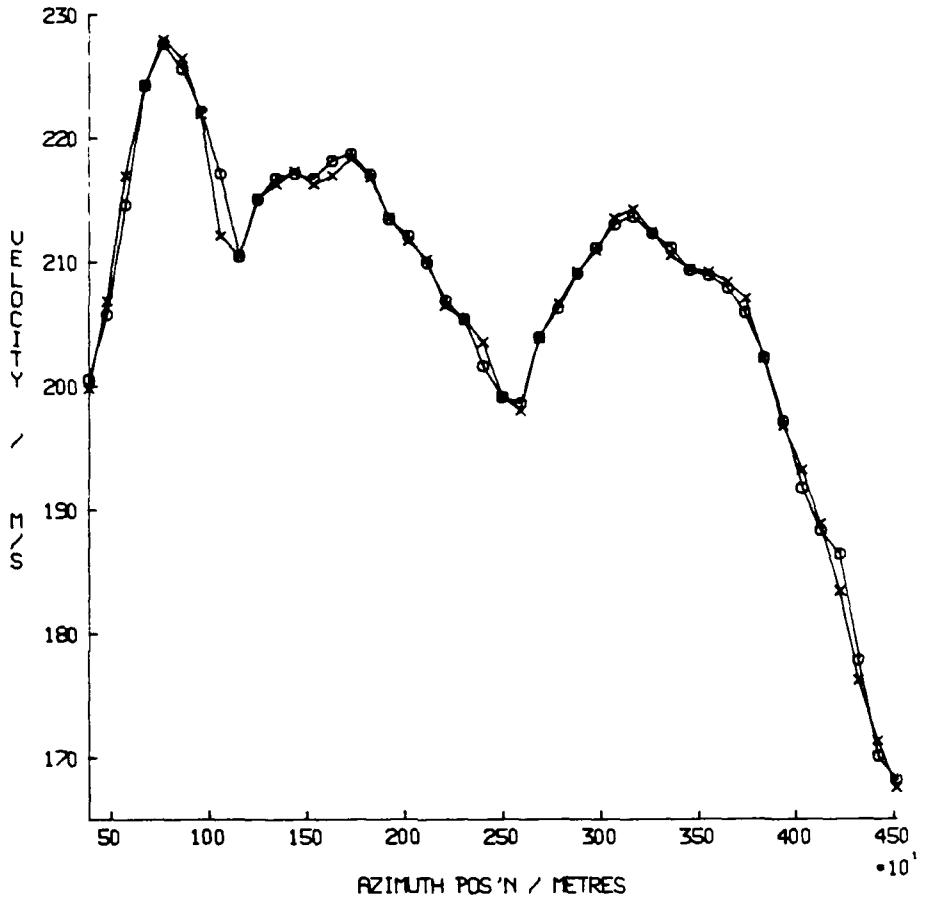

FIG 13 FORWARD AND BACKWARD VELOCITY PLOT USING MULTILOOK MISREGISTRATION AUTOFOCUS

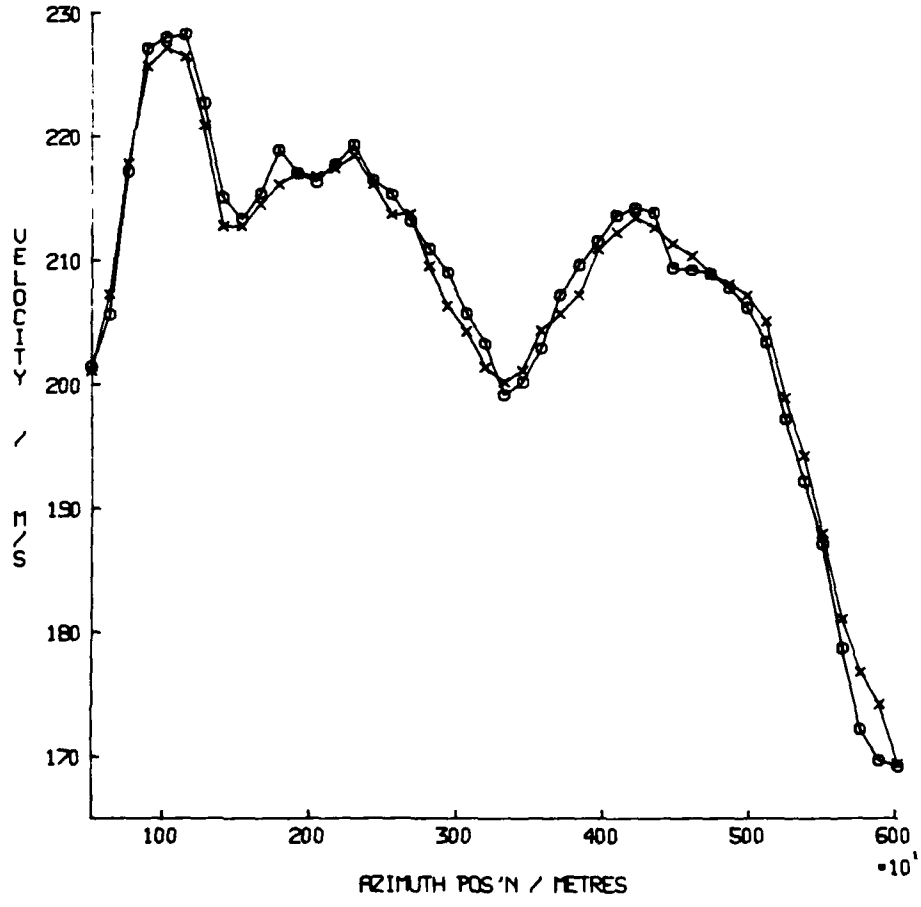

FIG 14 NEAR AND FAR SWATH VELOCITY PLOT USING CONTRAST OPTIMISED AUTOFOCUS

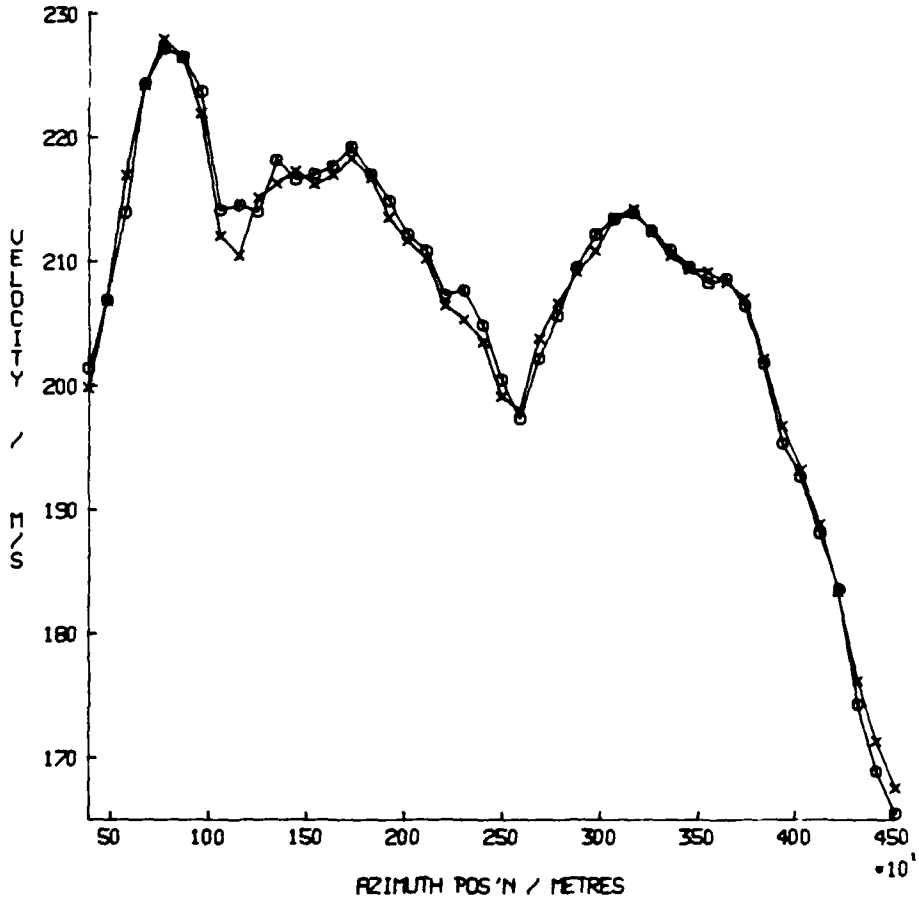

FIG 15 NEAR AND FAR SWATH VELOCITY PLOT USING MULTILOOK MISREGISTRATION AUTOFOCUS

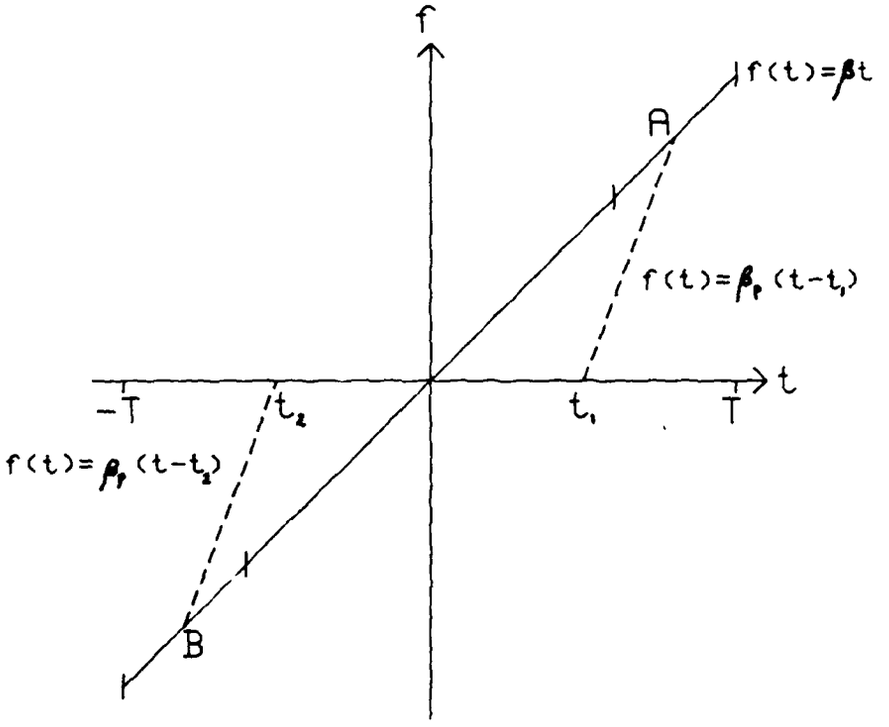

FIG. 16 MULTILOOK PROCESSING MISREGISTRATION

DOCUMENT CONTROL SHEET

Overall security classification of sheet .....UNCLASSIFIED.....

(As far as possible this sheet should contain only unclassified information. If it is necessary to enter classified information, the box concerned must be marked to indicate the classification eg (R) (C) or (S))

1. DRIC Reference (if known)	2. Originator's Reference	3. Agency Reference	4. Report Security Classification
	MEMORANDUM 3790	AD-A161912	U/C

5. Originator's Code (if known)	6. Originator (Corporate Author) Name and Location
	ROYAL SIGNALS AND RADAR ESTABLISHMENT
5a. Sponsoring Agency's Code (if known)	6a. Sponsoring Agency (Contract Authority) Name and Location

7. Title

AN INVESTIGATION OF SYNTHETIC APERTURE RADAR AUTOFOCUS

7a. Title in Foreign Language (in the case of translations)

7b. Presented at (for conference papers) Title, place and date of conference

8. Author 1 Surname, initials	9(a) Author 2	9(b) Authors 3,4...	10. Date	pp. ref.
FINLEY I P	WOOD J W			

11. Contract Number	12. Period	13. Project	14. Other Reference

15. Distribution statement

UNLIMITED

Descriptors (or keywords)

continue on separate piece of paper

Abstract

SAR imagery is generated by matched filtering the raw azimith signal history, assuming uniform straight line motion of the aircraft. Unknown aircraft motions alter the matched filter required for processing. Autofocussing involves determining from the raw data the appropriate matched filter.

In this memorandum the principles of SAR and the requirement for an autofocus system are discussed. Three autofocus methods are investigated: measurement of the power spectrum, contrast maximisation, and registration of multilook images. The power spectrum is shown to be unreliable as an autofocus aid. Results of the contrast maximisation and registration methods are compared.

END

DATE
FILMED

2-86

DTIC